Research Article

NMR IN BIOMEDICINE

Received: 15 January 2010, Revised: 30 July 2010, Accepted: 2 August 2010, Published online in Wiley Online Library: 19 October 2010

(wileyonlinelibrary.com) DOI:10.1002/nbm.1614

Quantitative magnetisation transfer imaging in glioma: preliminary results

Daniel J. Tozer[a]*, Jeremy H. Rees[a], Christopher E. Benton[a], Adam D. Waldman[a,b], H. Rolf Jäger[c] and Paul S. Tofts[a,d]

Quantitative magnetisation transfer imaging (qMTI) is an extension of conventional MT techniques and allows the measurement of parameters that reflect tissue ultrastructure through the properties of macromolecule-bound protons; these include the bound proton fraction and the relaxation times of free and bound proton pools. It has been used in multiple sclerosis and Alzheimer's disease, and has shown changes in some of the parameters, particularly the bound proton fraction. The purpose of this pilot study was to assess whether qMTI could distinguish between gliomas and normal brain tissue, and provide proof of principle for its use in tumour characterisation. Eight subjects [three men, five women; mean age, 44 years; range, 27–66 years; seven World Health Organization (WHO) Grade II, one Grade III] with biopsy-proven glioma were imaged with a structural MRI protocol that included three-dimensional qMTI. qMTI parameters were extracted from regions of interest selected from different tumour components visible on conventional MR sequences, normal-appearing peritumoral tissue and distant normal-appearing white matter. All patients gave informed consent and the study was approved by the Local Research Ethics Committee. Almost all of the qMTI parameters detected abnormalities in both glioma and the peritumoral region relative to the distant white matter. In particular, the bound proton fraction was reduced significantly from 6.0 percentage units (pu) [standard deviation (SD), 0.5 pu] in normal-appearing white matter to 1.7 pu (SD = 0.5 pu) in solid tumour and 2.2 pu (SD = 0.5 pu) in peritumoral areas. This work shows that qMTI reveals abnormalities, not only in glioma, but also in the apparently normal tissue surrounding the conventionally defined tumour. Thus, qMTI shows promise for tumour characterisation and for studying tumour boundaries. These preliminary data justify larger studies in a range of different tumour types and grades. Copyright © 2010 John Wiley & Sons, Ltd.

Keywords: glioma; quantitative magnetisation transfer; bound proton fraction; peritumoral tissue

INTRODUCTION

Low-grade gliomas are indolent primary brain tumours which may grow slowly for many years with minor symptoms; however, at an unpredictable time, the majority undergo malignant transformation into fatal high-grade tumours. 'Conventional' MRI using gadolinium-enhanced T_1- and T_2-weighted sequences is routinely used to image gliomas and provides information on the extent and location (1), but lacks biological specificity with regard to malignancy, histological subtype, the extent of tumour invasion into surrounding brain and therapeutic response. Physiological and quantitative MR techniques, such as perfusion and permeability imaging, *in vivo* spectroscopy and diffusion imaging, have shown potential for more specific tumour characterisation (2–4).

The phenomenon of magnetisation transfer (MT) (5) involves the exchange of magnetisation between protons in two pools: free protons in water molecules and bound protons attached to macromolecules within tissue. A mathematical model of MT, initially proposed by Henkelman *et al.* (6) and modified by Ramani *et al.* (7), has been developed; quantitative MT imaging (qMTI) can measure several fundamental and quantitative parameters related to MT (8,9) that reflect tissue ultrastructure. qMTI has been applied to patients with multiple sclerosis, where a decrease in the fraction of restricted protons (f_B) (potentially those in macromolecules, such as myelin) and an increase in the transverse relaxation time of restricted protons (T_{2B}) in multiple sclerosis lesions (8,10) have been seen. In Alzheimer's disease, f_B has also been shown to be reduced in the hippocampus (11). These results indicate that the technique is sensitive to pathology, which includes the destruction of the macromolecular structure of a tissue (reduction in f_B) or an increase in the free water content of the tissue [parameter gM_0^A; see eqn [1] below].

In gliomas, the macromolecular composition of the extracellular matrix differs from that of normal brain, and the tumour

* *Correspondence to: D. J. Tozer, Correspondence to: D. J. Tozer, NMR Research Unit, UCL Institute of Neurology, Queen Square, London WC1N 3BG, UK. E-mail: d.tozer@ion.ucl.ac.uk*

a *D. J. Tozer, J. H. Rees, C. E. Benton, A. D. Waldman, P. S. Tofts*
UCL Institute of Neurology, London, UK

b *A. D. Waldman*
Imperial College, London, UK

c *H. R. Jäger*
Lysholm Department of Neuroradiology, The National Hospital for Neurology and Neurosurgery, London

d *P. S. Tofts*
Brighton and Sussex Medical School, Falmer, Sussex, UK

Abbreviations used: *ANOVA, analysis of variance; APT, amide proton transfer; FLAIR, fluid attenuation inverse recovery; FSE, fast spin echo; MT(R), magnetisation transfer (ratio); NAWM, normal-appearing white matter; pu, percent unit; qMTI, quantitative magnetisation transfer imaging; SD, standard deviation; WHO, World Health Organization.*

may displace or destroy underlying brain microarchitecture; thus, it is likely that some qMTI parameters will be abnormal. Previous work has investigated the magnetisation transfer ratio (MTR) in both patients (12) and rats (13), and qMTI has been applied in rats (14) and in a single patient with a glioma (15).

The purposes of this preliminary work were to assess how qMTI parameters vary in gliomas relative to normal-appearing white matter (NAWM), and whether they show any promise as imaging biomarkers for these tumours.

EXPERIMENTAL DETAILS

Subjects

Eight patients were randomly recruited from the neuro-oncology clinic with histologically proven gliomas. The subjects consisted of three men and five women with an average age of 44 years [standard deviation (SD), 15 years; range, 27–66 years]. All subjects had biopsy or resection; in six cases this was after scanning; however, in two cases (one grade II oligodendroglioma and one grade II astrocytoma), biopsy was taken 4 years prior to scanning; the World Health Organization (WHO) grade and glioma subtype of the tumours were found to be grade II oligodendroglioma ($n = 3$), grade II astrocytoma ($n = 4$) and grade III anaplastic oligodendroglioma ($n = 1$). All patients gave written informed consent prior to scanning, and the study received ethical approval from the Local Research Ethics Committee.

MR imaging methods

Imaging was performed on a 1.5-T Signa MR scanner (GE Medical Systems, Milwaukee, WI, USA) using a birdcage (transmit–receive) head coil. After localisation scans, qMT images were acquired according to previously described methods (16). Four sequences were acquired; all were reconstructed to $28 \times 5\,mm^2$ slices with a field of view of $24 \times 24\,cm^2$ and a matrix of 256×256. The sequences acquired were as follows.

a) qMT images using the three-dimensional sequence described in ref. (16); this was a fast spoiled gradient echo sequence with TR/TE = 30.7/5.3 ms, an excitation flip angle of 5°, acquisition matrix of $256 \times 96 \times 32$ and acquisition field of view of $24 \times 18 \times 16\,cm^3$. MT saturation was achieved using a Gaussian pulse (SD = 2.83 ms; duration, 14.6 ms), applied once every TR prior to radiofrequency excitation. Ten MT-weighted datasets were collected using two MT pulse amplitudes (described by their equivalent on-resonance flip angles: 212° and 843°). For each amplitude, five frequency offsets, ranging from 400 Hz to 20 kHz, separated by a constant logarithmic step of ~ 0.4, were used (16).

b) Three three-dimensional spoiled gradient echo volumes with TR/TE = 13.1/4.2 ms and excitation flip angles α of 25°, 15° and 5°, to estimate T_1.

c) Fast spin echo (FSE) fluid attenuation inverse recovery (FLAIR) images with TR/TI/TE = 8774/2192/161 ms.

d) FSE images with TR/TE = 5000/81 ms and an echo train length of 8.

Image analysis

Images were transferred to a Unix workstation (Sun Microsystems, Mountain View, CA, USA) for further processing. For each subject, the first qMTI dataset (i.e. 400 Hz offset and on-resonance equivalent flip angle of 212°) was used as a base, and the subsequent qMTI, FLAIR and FSE data were registered to it using a normalised mutual information cost function (17). Regions of interest were identified for each subject by an experienced rater on the registered FLAIR images for contralateral NAWM, whole tumour and solid tumour. FLAIR images were used as they provide the best delineation of the tumour from surrounding brain tissue; the FSE images were also used as a visual reference when drawing the regions, as the different contrast can aid in tissue delineation. The whole tumour was delineated on all slices and may have included small cystic areas, with only large cysts excluded from the region of interest. Solid tumour was defined as a region of the whole tumour free of all visible cysts. To calculate the peritumoral area, this whole tumour region was dilated by 5 pixels (a distance of approximately 5 mm). This dilated region of interest was combined with a white matter mask derived from SPM5 (Wellcome Department of Cognitive Neurology, UCL Institute of Neurology, London, UK), by segmenting the first qMTI dataset into white matter, grey matter and cerebrospinal fluid and then using a lower threshold of 75% to generate a final white matter segment, with the original tumour region subtracted to leave only the NAWM surrounding the tumour. Figure 1 shows an example of one slice of one of the tumours with the regions of interest superimposed on it.

These multislice regions were then analysed to produce the qMTI parameters described below, and the mean value of each of the parameters was then obtained and compared between the tissues. In addition, pixel-by-pixel maps of the qMTI parameters were produced for each subject to investigate the heterogeneity of the tumour.

The parameter values were estimated using eqns [1] and [2] and the super-Lorentzian lineshape [3], which was used for the absorption lineshape of the bound protons (R_{RFB}):

$$S = gM_0^A\left(\frac{R_B\left[\frac{RM_0^A f_B}{R_A(1-f_B)}\right] + R_{RFB} + R_B + RM_0^A}{\left[\frac{RM_0^A f_B}{R_A(1-f_B)}\right](R_B + R_{RFB}) + \left(1 + \left[\frac{\omega_{CWPE}}{2\pi\Delta f}\right]^2\left[\frac{1}{R_A T_{2A}}\right]\right)(R_{RFB} + R_B + RM_0^A)}\right) \quad [1]$$

$$R_{RFB} = \pi\omega_{CWPE}{}^2 G_{SL}(2\pi\Delta f) \quad [2]$$

$$G_{SL}(2\pi\Delta f) = \int_0^{\frac{\pi}{2}} d\theta \sin\theta \sqrt{\frac{2}{\pi}} \frac{T_{2B}}{\left(\left|3\cos^2\theta - 1\right|\right)} e^{-2\left[\frac{2\pi\Delta f T_{2B}}{\left|3\cos^2\theta-1\right|}\right]^2} \quad [3]$$

In eqn [1], S is the signal intensity obtained from a volume of interest, g is a scaling factor based on the electronic settings of the scanner, M_0^A is the native magnetisation of the free pool, R_A

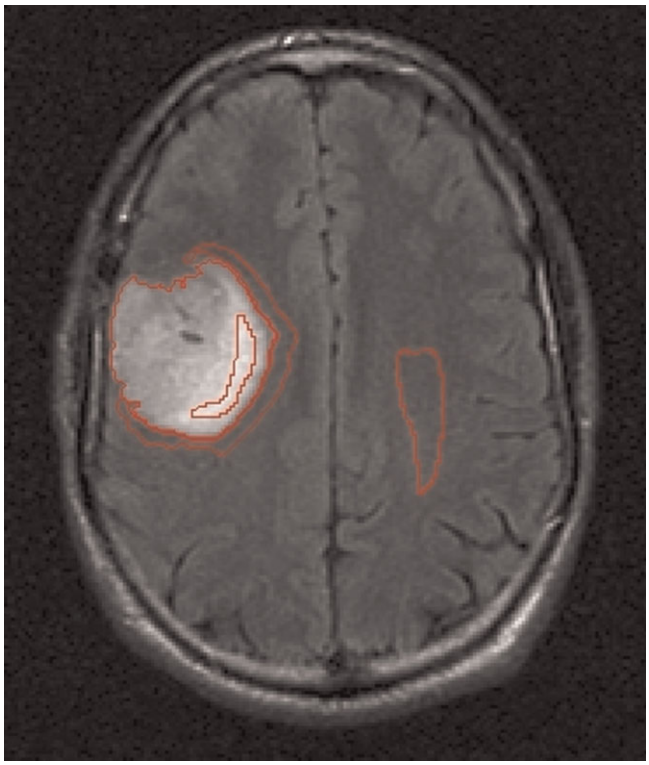

Figure 1. A slice from one of the subjects showing the tumour as the bright area on the left-hand side of the image. Also shown are the various regions of interest. The region on the right of the image is the normal-appearing white matter. The peritumoral region can be seen as the crescent surrounding the large tumour region, and the area of solid tumour is the region drawn within the whole tumour region.

and R_B are the longitudinal relaxation rates of the free (A) and bound (B) pools, respectively (measured in Hz) (where, as in previous work, R_B is fixed at unity), R is the cross-relaxation rate between the two pools (Hz), T_{2A} and T_{2B} are the transverse relaxation times (s) of the two pools, f_B is the bound proton fraction (% or percent units, pu) and Δf is the offset frequency of the pulse (Hz); ω_{CWPE} is the continuous wave power equivalent amplitude of the saturation pulse (rad/s), and describes the saturating effect of the MT pulse, which is used instead of a continuous wave saturation for which the original model was developed (18). The model was fitted to the data using the Levenberg–Marquardt algorithm, as described in ref. (16), to produce estimates of the following parameters: gM_0^A; RM_0^A; $1/R_AT_2^A$; $f_B/R_A(1-f_B)$ and T_2^B. From these estimates, the value of T_{1obs} obtained using the three three-dimensional volumes described earlier ($= 1/R_{1obs}$) and eqn [4]:

$$R_A = \frac{R_{1\,obs}}{1+\left(\frac{\frac{RM_0^A f_B}{(1-f_B)R_A}(R_B-R_{1\,obs})}{(R_B-R_{1\,obs})+RM_0^A}\right)} \qquad [4]$$

values for R_A, f_B and T_{2A} can be obtained.

Statistical methods

For each of the qMTI parameters, an analysis of variance (ANOVA) was carried out to establish whether there were differences between the means extracted from the contralateral NAWM, the whole tumour, the solid tumour and the peritumoral white matter. For each of the tissue qMTI parameters with $p < 0.05$ (from the ANOVA test, indicating that the parameter varies between the tissue means), each pair of tissues was tested using Student's paired *t*-test and corrected for multiple comparisons using the Bonferroni correction.

RESULTS

Figure 2 shows an example FLAIR image and corresponding qMTI parameter maps for one of the subjects. This subject has a cystic area as well as a solid tumour. It can be seen that the parameters behave differently with regard to the different tissues. For example, the f_B map illustrates that the whole tumour shows a large reduction in the bound proton fraction, whereas the reduction in T_{2B} appears to be greater in the cystic areas, which corresponds to the same area showing the largest increase on T_{1obs}, T_{1A} and T_{2A} maps.

qMTI parameter estimates were obtained from contralateral NAWM, whole tumour, solid tumour and peritumoral white matter in all eight subjects. The region volume for each of the tissues (mean $\pm$ SD) was 3.7 ± 1.7 mL for contralateral white matter, 87.8 ± 47.7 mL for the whole tumour, 2.5 ± 1.4 mL for solid tumour and 12.3 ± 4.4 mL for peritumoral white matter. The individual regional volumes are shown in Table 1, together with the histological data.

Table 2 shows the qMTI parameter values for each tissue from the region of interest analysis. ANOVA showed significant differences ($p < 0.001$) between the tissues analysed for T_{1obs}, RM_0^A, $f_B/R_A(1-f_B)$, T_{2B}, $1/R_AT_{2A}$, R_A, f_B and T_{2A}. The results of Student's paired *t*-test for comparison of the tissues are shown in Table 3. Figure 3 illustrates a box-plot representation of the f_B values, showing the difference in the range of values for this parameter for the various tissue types.

Significant differences between solid tumour and NAWM were seen for many of the parameters, even allowing for the correction for multiple comparisons (Table 3). Two of the qMTI parameters (as well as T_{1obs}) showed differences between the peritumoral region, beyond the margin of abnormality on FLAIR imaging, and distant white matter, suggesting that, although normal appearing, the peritumoral region is, in fact, abnormal. This suggests that this tissue is already undergoing some pathological changes, even though it is not formally defined as tumour. However, there were still significant differences between the tumour and peritumoral tissue, indicating that the tissue is not yet as extremely affected as the tumour. There was no difference between the whole tumour and solid tumour.

DISCUSSION

As far as we are aware, apart from a single subject described by Yarnykh (15), this is the first qMT study of human brain gliomas. Although the number of patients is limited, significant differences were shown between NAWM, tumour and peritumoral tissue. Although Yarnykh (15) used different imaging and modelling methods, the patient described showed similar parameter changes to those found here, such that the fraction of bound protons was reduced significantly in the tumour compared with white matter. Similarly, a study of qMTI in gliomas implanted to mice (14) also showed a reduction in the percentage of bound

NMR IN BIOMEDICINE

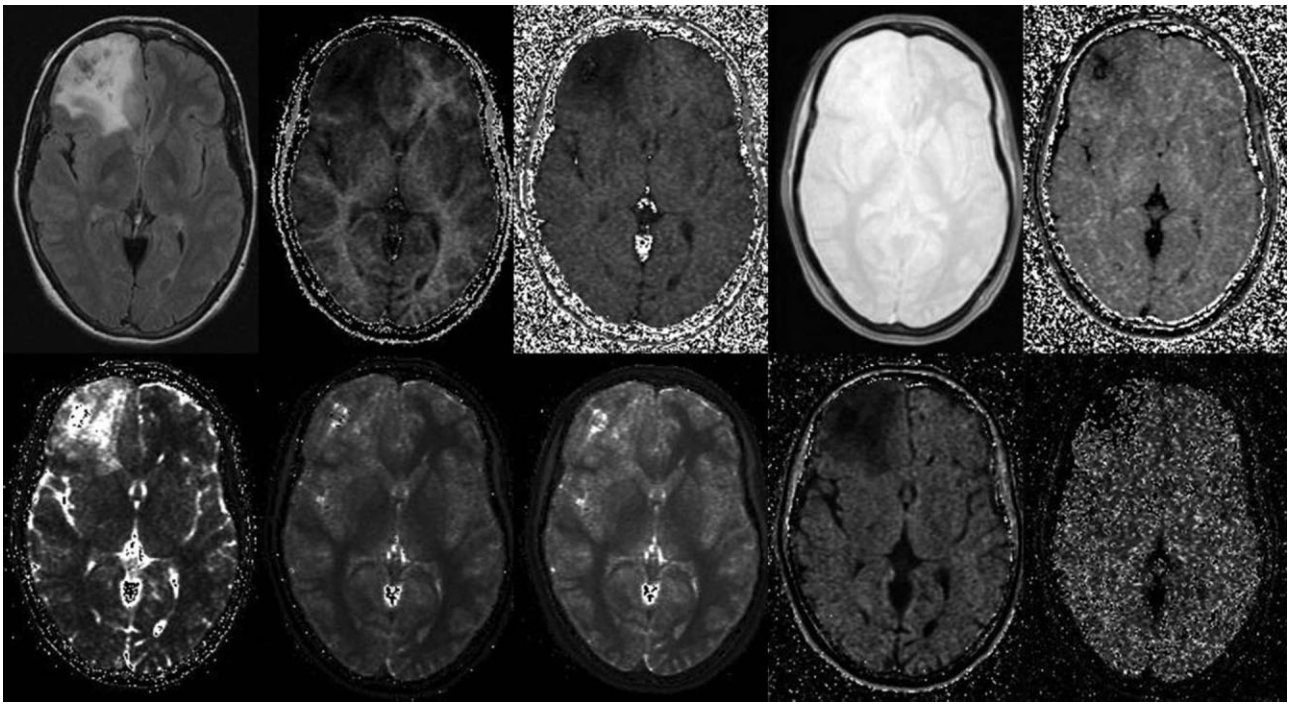

Figure 2. Images and parameter maps for a subject with an anaplastic oligodendroglioma. The images are (from left to right, top then bottom row): fluid attenuation inverse recovery (FLAIR) image (fast spin echo FLAIR image, axial plane, TR/TI/TE = 8774/2192/161 ms), f_B, $f/R_A(1 - f_B)$, gM_0^A, T_{2B}, T_{2A}, T_{1A}, T_{1obs}, $1/R_AT_{2A}$ and RM_0^A (all calculated parameter maps in the axial plane). The tumour is visible in the top left corner of the brain (as viewed), and most parameters show abnormalities in the tumour and heterogeneity within it.

Table 1. Regional volumes for the individual subjects. The regional volumes indicate the size of the region drawn in the given tissue and not the total volume of that tissue within the tumour

Patient	Histology (WHO grade)	White matter (mL)	Solid tumour (mL)	Whole tumour (mL)	Peritumoral white matter (mL)
1	O (II)	4.4	1.5	75.2	9.3
2	A (II)	2.0	1.5	68.9	9.6
3	O (II)	3.2	5.5	185.6	19.7
4	AO (III)	2.5	2.9	70.6	7.8
5	A (II)	7.2	1.9	45.6	10.2
6	A (II)	3.4	2.6	84.8	15.2
7	O (II)	4.6	1.2	42.3	9.6
8	A (II)	2.3	2.7	128.7	17.1

A, astrocytoma; AO, anaplastic oligodendroglioma; O, oligodendroglioma; WHO, World Health Organization.

Table 2. Quantitative magnetisation transfer imaging (qMTI) parameter values from the various tissues analysed. Mean over all subjects, derived from means of all regions within each subject, ± standard deviation across subjects

	T_{1obs} (ms)	RM_0^A	$f_B/R_A(1 - f_B)$	T_{2B} (μs)	$1/R_AT_{2A}$	gM_0^A	R_A (s^{-1})	f_B (pu)	T_{2A} (ms)
White matter	838 ± 59	85 ± 16	0.053 ± 0.004	8.8 ± 0.5	10.1 ± 1.2	509 ± 123	1.21 ± 0.08	6.0 ± 0.5	83 ± 10
Whole tumour	2135 ± 593	183 ± 110	0.030 ± 0.005	6.6 ± 0.7	5.8 ± 0.9	580 ± 145	0.49 ± 0.11	1.4 ± 0.5	389 ± 174
Solid tumour	1878 ± 326	91 ± 32	0.032 ± 0.006	7.6 ± 0.9	5.5 ± 0.7	599 ± 152	0.54 ± 0.09	1.7 ± 0.5	351 ± 83
Peritumoral white matter	1044 ± 113	75 ± 18	0.049 ± 0.006	8.6 ± 0.5	10.0 ± 1.0	534 ± 133	0.97 ± 0.11	4.5 ± 0.8	106 ± 19

pu, percent unit.

Table 3. *p* values from a comparison of the tissues using Student's paired *t*-test. *p* values in bold are significant after Bonferroni correction for multiple comparisons (effective *p* value for significance, 0.0012)

		T_{1obs}	RM_0^A	$f_B/R_A(1-f_B)$	T_{2B}	$1/R_AT_{2A}$	R_A	f_B	T_{2A}
White matter	Whole tumour	**0.0005**	0.035625	$\mathbf{7\times10^{-6}}$	$\mathbf{5\times10^{-5}}$	$\mathbf{3\times10^{-5}}$	$\mathbf{9\times10^{-7}}$	$\mathbf{2\times10^{-7}}$	0.002
	Solid tumour	$\mathbf{3\times10^{-5}}$	0.631309	$\mathbf{1\times10^{-5}}$	0.003	$\mathbf{6\times10^{-6}}$	$\mathbf{2\times10^{-7}}$	$\mathbf{2\times10^{-7}}$	$\mathbf{4\times10^{-5}}$
	Peritumoral white matter	**0.0003**	0.107191	0.035	0.35	0.81	**0.0001**	**0.0002**	0.005
Whole tumour	Solid tumour	0.077	0.025745	0.029	0.002	0.286	0.077	0.009	0.437
	Peritumoral white matter	**0.0012**	0.017057	$\mathbf{1\times10^{-5}}$	$\mathbf{4\times10^{-5}}$	$\mathbf{4\times10^{-5}}$	$\mathbf{3\times10^{-5}}$	$\mathbf{1\times10^{-5}}$	0.003
Solid tumour	Peritumoral white matter	$\mathbf{8\times10^{-5}}$	0.062353	$\mathbf{1\times10^{-5}}$	0.005	$\mathbf{2\times10^{-7}}$	$\mathbf{3\times10^{-6}}$	$\mathbf{3\times10^{-6}}$	$\mathbf{3\times10^{-5}}$

protons, as well as a reduction in T_{2B} and changes in other parameters. Again the model used in ref. (14) is not directly comparable with that used here and the tissues studied were not identical; however, the results seen in ref. (14) were broadly the same as those presented here. The results seen here can also be compared with studies applying MTR to gliomas. Both refs. (12) and (13) found a reduction in MTR in tumour compared with white matter, suggesting either a reduction in the bound proton fraction or an increase in T_1. Although the acquisition and processing of qMT data is more complex than magnetisation transfer ratios (MTR), it may be more sensitive to pathology. MTR is approximately proportional to both f_B and T_1 (19); thus, the changes seen in these parameters will tend to counteract each other, effectively reducing the sensitivity of the technique. For example, ref. (14) shows an increase in T_{1A} in the tumour of approximately 26% and a decrease in M_0^B, equivalent to f_B, of approximately 65% compared with white matter; the change seen in the parameter Max MT, an analogue of MTR, is only approximately 12%, much less than that seen in the qMTI parameters.

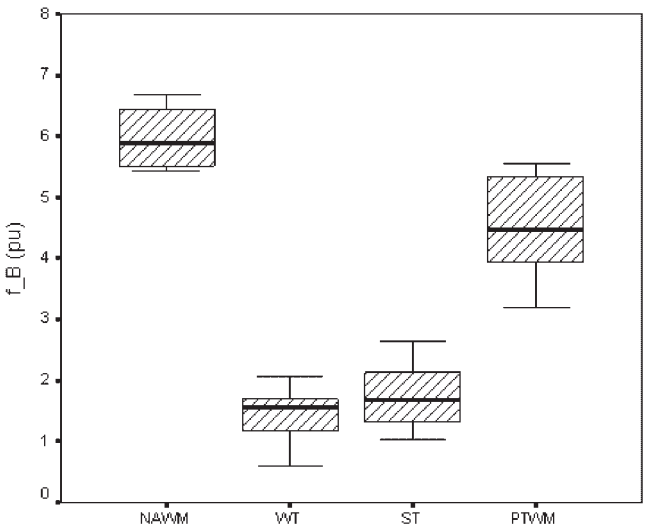

Figure 3. Boxplot showing the f_B values for the normal-appearing white matter (NAWM), whole tumour (WT), solid tumour (ST) and peritumoral white matter (PTWM). The full line indicates the median value, the box the interquartile range and the whiskers the extreme values. The graph shows the reduction in f_B in the tumour and PTWM compared with NAWM.

Another related technique that has been used in gliomas is that of amide proton transfer (APT), which is similar to MTR except that the amide protons with a resonance around 3.5 ppm downstream from the water resonance are specifically targeted, rather than the bound protons in macromolecules. Work in patients (20) and rats (21) with glioma has shown an increased APT ratio in the tumour compared with normal tissue, and good contrast between the tumour and white matter on APT-weighted images. These results indicate an increase in protein/peptide content in the tumour (20), which outweighs any increase in water. This is in contrast with the results presented in this work, where a reduction in bound protons in macromolecules is seen, and which works with any increase in water content.

Although ANOVA showed no significant difference in proton density (i.e. gM_0^A) across tissue types, indicating no increase in water content in the tumour, such an increase has been seen previously (22). R_A is reduced in gliomas, which implies an increased T_{1A}; an increase in the observed T_1 value has been shown in these results and previously (23), and is probably a result of an increase in water content. Interestingly, peritumoral tissue also shows similar effects, possibly indicating inflammation surrounding the tumour proper, although there is no significant change in the proton density.

T_{2A} is also highly increased in solid tumour, again probably a result of extra water in the tissue. The small reduction in T_{2B} appears to be concentrated in cystic areas and is not altered significantly in solid tumour. This suggests that the macromolecular protons lost in the tumour are not of one specific species, with a characteristic T_2, whereas, in cystic areas, either the excess fluid alters the T_2 of the bound protons or the remaining bound protons belong to macromolecules with a subset of T_2 times. The bound proton fraction f_B is reduced, probably because of the destruction of macromolecules by the tumour cells, or as a function of increased water content, and this seems to occur throughout the tumour. The bound proton fraction in the tumour is reduced to less than one-third of the value in white matter; this compares with an increase in the proton density of around 20% in the tumour. Thus, there is a reduction in the absolute concentration of bound protons in the tissue, as well as an increase in the absolute concentration of free protons in the tumour.

Although there is no histological evidence, the abnormal qMT parameters in the peritumoral region (despite no significant change in the proton density) indicate that the tumour boundary, as conventionally defined on anatomical images such as FLAIR,

underestimates the limit of tissue pathology. This is in agreement with work using diffusion parameters, such as the mean diffusivity and fractional anisotropy, which found abnormalities in the peritumoral region (24–26) in high-grade gliomas, and has implications for the planning of maximal surgical resection and radiotherapy treatment.

Although Fig. 2 shows parameter maps for the only subject with a grade III glioma, the pixel-by-pixel maps and region of interest analyses do not differ from those of low-grade gliomas – each parameter falls within the range of the other seven subjects, and therefore it is reasonable to include this subject in the analysis. Further analysis of a larger number of subjects should investigate the difference between high- and low-grade gliomas, and also the histological subtypes of glioma, which was not performed here because of the small number of subjects.

Another area worthy of discussion is the choice of tissue in the regions of interest. These were drawn on the FLAIR images by hand, which may introduce a subjective element to the process. However, as the regions were then transferred to the qMT parameter maps for analysis (which are independent of the FLAIR images), this effect is minimised. Similarly, the choice of five dilations for the study of the peritumoral region is arbitrary. However, the results seem to indicate abnormalities in the tissue outside of the FLAIR-defined tumour, with Fig. 3 showing that f_B is reduced towards the values seen in the tumour proper. These results may warrant further study to determine the extent and gradient of these parameter changes.

Although the results presented here do not attempt to differentiate between low- and high-grade glioma, it should be noted that the histology presented above may be of limited value. Firstly, sampling error may mean that tumours are of a higher grade than determined from a biopsy. Most importantly, tumours may change grade rapidly; although this is not an issue for the six tumours biopsied or resected after scanning, it may have occurred in the other two subjects. These subjects were examined radiologically and clinically every 6 months, and no changes were noted after biopsy to a period of at least 2 years after scanning; therefore, it is unlikely that the tumours had progressed, but it remains a possibility.

The small variation in the parameters in NAWM suggests that the fitting techniques used are reliable. The fact that the percentage variation for all parameters is higher in pathological tissues suggests that biological variation is greater than that introduced by the nonlinear model used. This may explain why the increase in variation in f_B relative to T_{1obs} is smaller than expected from the nonlinearity of eqns [1] and [4].

When compared with the values for NAWM seen in multiple sclerosis (10), the values presented here differ, in particular with regard to the f_B values. There are a number of possible reasons for this. Firstly, the sequence used here is not the two-dimensional sequence used in ref. (10), and the data points acquired also differ in terms of MT pulse power and frequency offset, which may lead to the different parameter estimates. Secondly, the T_1 calculation method used also differs from that employed in the previous work, and there is a difference in the estimates of T_1 in the two studies, as well as in the qMT parameters. Thirdly, the scanner underwent a software upgrade between the studies, which may also have contributed to the differences seen in the parameter values. All of these technical issues raise questions about the use of qMT to obtain scanner/sequence-independent biologically meaningful measurements, and it is true that further study of the technique is required to show that this is possible. The other possible explanation for the differences is that the white matter studied here has a diffuse pathology, causing it to be abnormal compared with control white matter, although this seems unlikely given the scale of the differences seen between this work and ref. (10), and what is known about the normal brain in glioma.

Future areas of work may include a study of the spatial distribution of the qMT parameters (for example, using measures of heterogeneity, such as histograms and texture), and further analysis of the tissues within the tumour, correlation of the parameters with histological subtype and the study of parameter changes with regard to malignant transformation.

The abnormalities seen in the peritumoral region are probably the most surprising aspect of this work. The changes seen in this region relative to NAWM suggest that there may be pathological processes occurring, which may have implications for tissue preservation during surgery. In conclusion, these preliminary results indicate that qMTI probably has some value in the imaging of gliomas, in the context of understanding tumour biology, treatment trials and monitoring of individual responses to treatment.

qMTI investigates the relationship between bound and free protons in a tissue, which can provide information on the level of fluid or tissue breakdown within the tumour. This is in contrast with other quantitative MR techniques used in gliomas, such as perfusion and permeability imaging, which investigate the vascularity and blood–brain barrier breakdown, respectively. These aspects of glioma development are very different and the methods may therefore provide complementary information. qMT is more similar to diffusion analysis, in that the apparent diffusion coefficient and fractional anisotropy will be affected by an increase in fluid and the destruction of tissue structures, so that the two methods may be more correlated, although studies need to be performed to address this. With regard to conventional imaging techniques used in gliomas, quantitative MR techniques, such as qMTI, can provide information on specific aspects of tissue biology and pathology, and can yield reproducible measures for the study of longitudinal changes, which cannot be obtained from conventional images.

Acknowledgements

This work and CEB were funded by the Samantha Dickson Brain Tumour Trust (grant number 22.03). DJT was funded by a grant from the Multiple Sclerosis Society of Great Britain and Northern Ireland.

REFERENCES

1. Keeles GE, Berger MS. Advances in neurosurgical technique in the current management of brain tumors. Semin. Oncol. 2004; 31: 659–665.
2. Waldman AD, Jackson A, Price SJ, Clark CA, Booth TC, Auer DP, Tofts PS, Collins DJ, Leach MO, Rees JH. Quantitative imaging biomarkers in neuro-oncology. Nat. Rev. Clin. Oncol. 2009; 6: 445–454.
3. Cha S, Tihan T, Crawford F, Fischbein NJ, Chang S, Bollen A, Nelson SJ, Prados M, Berger MS, Dillon WP. Differentiation of low-grade oligodendrogliomas from low-grade astrocytomas by using quantitative blood-volume measurements derived from dynamic susceptibility contrast-enhanced MR imaging. Am. J. Neuroradiol. 2005; 26: 266–273.

4. Sugahara T, Korogi Y, Kochi M, Ikushima I, Shigematu Y, Hirai T, Okuda T, Liang LX, Ge YL, Komohara Y, Ushio Y, Takahashi M. Usefulness of diffusion-weighted MRI with echo-planar technique in the evaluation of cellularity in gliomas. J. Magn. Reson. Imaging, 1999; 9: 53–60.
5. Wolff SD, Balaban RS. Magnetization transfer contrast (MTC) and tissue water proton relaxation in vivo. Magn. Reson. Med. 1989; 10: 135–144.
6. Henkelman RM, Huang X, Xiang Q, Stanisz GJ, Swanson SD, Bronskill MJ. Quantitative interpretation of magnetization transfer. Magn. Reson. Med. 1993; 29: 759–766.
7. Ramani A, Barker GJ, Dalton C, Miller DH, Tofts PS. Precise estimate of fundamental *in-vivo* MT parameters in human brain in clinically feasible times. Magn. Reson. Imaging, 2002; 20: 721–731.
8. Tozer D, Ramani A, Barker GJ, Davies G, Miller DH, Tofts PS. Quantitative magnetisation transfer mapping of bound protons in multiple sclerosis. Magn. Reson. Med. 2003; 50: 83–91.
9. Sled JG, Pike GB. Quantitative imaging of magnetization transfer exchange and relaxation properties in vivo using MRI. Magn. Reson. Med. 2001; 46: 923–931.
10. Davies GR, Tozer DJ, Cercignani M, Ramani A, Dalton C, Thompson AJ, Barker GJ, Tofts PS, Miller DH. Estimation of the macromolecular proton fraction and bound pool T_2 in multiple sclerosis. Multiple Sclerosis, 2004; 10: 607–613.
11. Ridha BH, Tozer DJ, Symms MR, Stockton KC, Lewis EB, Siddique MM, MacManus DG, Rossor MN, Fox NC, Tofts PS. Quantitative magnetization transfer imaging in Alzheimer's disease. Radiology, 2007; 244: 832–837.
12. Lemaire L, Franconi F, Saint-André JP, Roullin V-G, Jallet P, Lw Jeune J-J. High-field quantitative transverse relaxation time, magnetisation transfer and apparent water diffusion in experimental rat brain tumour. NMR Biomed. 2000; 13: 116–123.
13. Kurki T, Lundbom N, Kalimo H, Valtonen S. MR classification of brain gliomas: value of magnetization transfer and conventional imaging. Magn. Reson. Imaging, 1995; 13: 501–511.
14. Quesson B, Bouzier A-K, Thiaudiere E, Delalande C, Merle M, Canioni P. Magnetization transfer fast imaging of implanted glioma in the rat brain at 4.7 T: interpretation using a binary spin-bath model. J. Magn. Reson. Imaging, 1997; 7: 1076–1083.
15. Yarnykh VL. Pulsed Z-spectroscopic imaging of cross-relaxation parameters in tissues for human MRI: theory and clinical applications. Magn. Reson. Med. 2002; 47: 929–939.
16. Cercignani M, Symms MR, Schmierer K, Boulby PA, Tozer DJ, Ron M, Tofts PS, Barker GJ. Three-dimensional quantitative magnetisation transfer imaging of the human brain. Neuroimage, 2005; 27: 436–441.
17. Studholme C, Hill DLG, Hawkes DJ. An overlap invariant entropy measure of 3D medical image alignment. Pattern Recogn. 1999; 32: 71–86.
18. Ramani A, Tofts PS. Comparison of continuous wave theory to pulsed multicentre MT data. *Proceedings of the 8th Annual Meeting ISMRM*, Denver, CO, USA 2000; 2078.
19. Tofts PS, Steens SCA, van Buchem MA. MT: magnetisation transfer. In: *Quantitative MRI of the Brain: Measuring Changes Caused by Disease*, Tofts PS (ed). John Wiley: Chichester, 2003; 256–298.
20. Jones CK, Schlosser MJ, van Zijl PCM, Pomper MG, Golay X, Zhou J. Amide proton transfer imaging of human brain tumors at3T. Magn. Reson. Med. 2006; 56: 585–592.
21. Zhou J, Lal B, Wilson DA, Laterra J, van Zijl PCM. Amide proton transfer (APT) contrast for imaging of brain tumors. Magn. Reson. Med. 2003; 50: 1120–1126.
22. Just M, Thelen M. Tissue characterization with T1, T2, and proton density values – results in 160 patients with brain-tumors. Radiology, 1988; 169: 779–785.
23. Englund E, Brun A, Larsson EM, Gyorffy-Wagner Z, Persson B. Tumours of the central nervous system. Proton magnetic resonance relaxation times T1 and T2 and histopathologic correlates. Acta Radiol. Diagn. 1986; 27: 653–660.
24. Provenzale JM, McGraw P, Mhatre P, Guo AC, Delong D. Peritumoral brain regions in gliomas and meningiomas: investigation with isotropic diffusion-weighted MR imaging and diffusion-tensor MR imaging. Radiology, 2004; 232: 451–460.
25. Lu S, Ahn D, Johnson G, Law M, Zagzag D, Grossman RI. Diffusion-tensor MR imaging of intracranial neoplasia and associated peritumoral edema: introduction of the tumor infiltration index. Radiology, 2004; 232: 221–228.
26. Lin CP, Guo WY, Chou KH, Chen MT, Chen MH, Yen YS, Chao YP, Ho DMT. Peri-tumoral fractional anisotropy mapping as a prognosticator and treatment guidance of brain tumors: a feasibility study. J. Med. Biol. Eng. 2008; 28: 139–145.